GEOPHYSICS, VOL. 38, NO. 3 (JUNE 1973), P. 581–599, 17 FIGS.

RADIO INTERFEROMETRY DEPTH SOUNDING: PART II—EXPERIMENTAL RESULTS†

JAMES R. ROSSITER*, GERALD A. LATORRACA‡, A. PETER ANNAN*, DAVID W. STRANGWAY*§, AND GENE SIMMONS‡

In such highly resistive geologic environments as ice sheets, salt layers, and the moon's surface, radio waves penetrate with little attenuation. The field strengths about a transmitting antenna placed on the surface of such an environment exhibit interference maxima and minima which are indicative of the in-situ electrical properties and the presence of subsurface layering.

Experimental results from an analog scale model and from field tests on two glaciers are interpreted on the basis of the theoretical results of Part I. If the upper layer is thick, the pattern is very simple and the dielectric constant of the layer can be easily determined. An upper bound on the loss tangent can be estimated. For thin layers, the depth can be determined if the loss tangent is less than about 0.10, and a crude estimate of scattering can be made.

INTRODUCTION

The attenuation of electromagnetic waves propagating through terrestrial rocks is extremely high due to the moisture content; as a result, EM methods in the radio-frequency range have not found general use in exploring the earth. A few highly resistive geologic environments, such as ice sheets (Evans, 1963, 1965, 1967; Jiracek, 1967) and dry salt layers (Unterberger et al, 1970; Holser et al, 1972), are sufficiently dry to be transparent to radio waves. The uppermost layers of the moon are also very resistive (Strangway, 1969; Saint-Amant and Strangway, 1970), and typical attenuation distances (or skin depths) for lunar material are shown in Figure 1.

In these materials, EM waves propagate with little attenuation and are useful, in theory, for depth sounding. The Surface Electrical Properties Experiment, which was developed for Apollo 17, uses such a method to measure the electrical properties of the moon and to search for layering. The method is based on the interference pattern generated between various radio waves.

Theoretical background to the method and a general introduction to this series of papers is presented in Part I by Annan (1973, p. 557). In preparation for interpretation of lunar data, we have tested the method both in the laboratory with analog scale models using wavelengths in the centimeter range and in the field on glaciers using wavelengths about the same as will be used on the moon. These results are presented here.

INTERFEROMETRY TECHNIQUE

Radio-frequency interferometry (RFI) is described simply as follows: A transmitter and associated antenna on the dielectric surface generate RF waves which are received and amplified at some distance. Several waves reach the receiver —e.g., A, B, and C shown in Figure 2. Because the various waves travel different distances and/or at different velocities, they interfere with each other. The interference pattern can be generated in one of two different ways. Either frequency or distance can be varied, holding the other constant. Frequencies of 500 khz to 50 Mhz and distances

† Presented at the 40th Annual International SEG Meeting, November 9, 1970, New Orleans, Louisiana. Manuscript received by the Editor April 6, 1972; revised manuscript received November 22, 1972.

* University of Toronto, Toronto 181, Ontario, Canada.

‡ Massachusetts Institute of Technology, Cambridge, Massachusetts 02139.

§ Presently on leave to NASA Manned Spacecraft Center, Houston, Texas 77058.

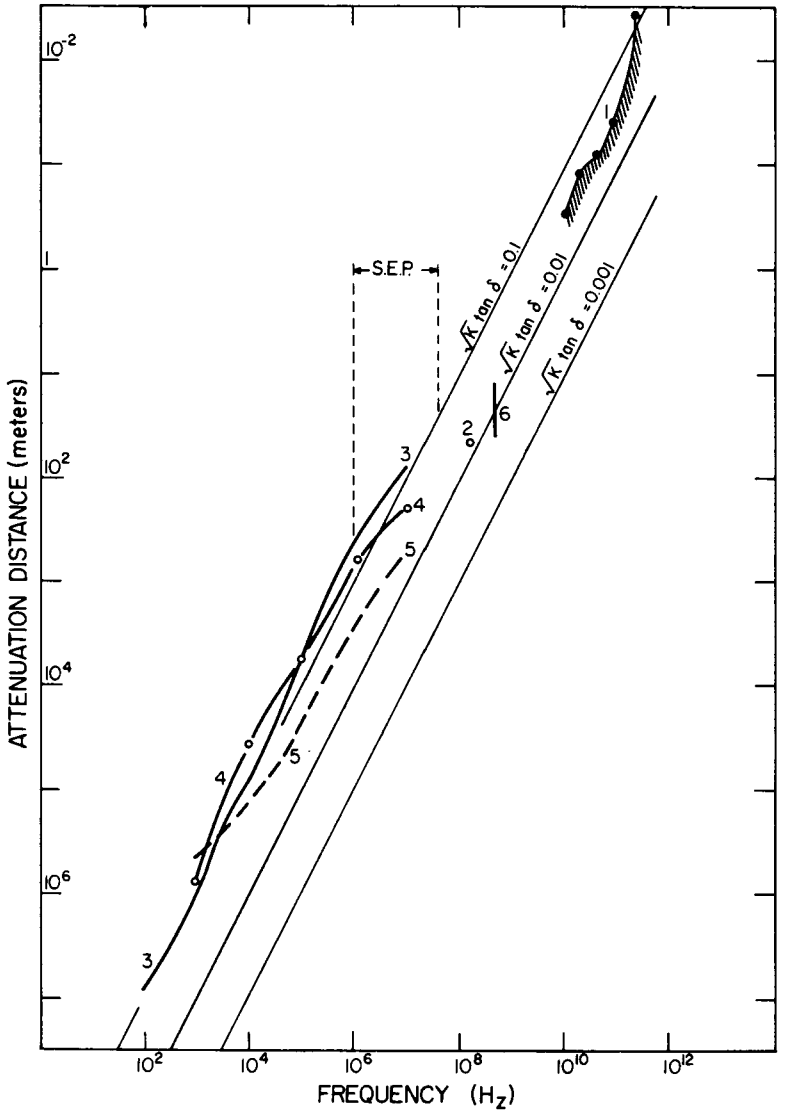

FIG. 1. Attenuation distance in lunar surface material: 1. Weaver (1965)—thermal emission; 2. Tyler (1968)—bistatic radar; 3. Chung et al (1971)—igneous sample 12002,58; 4. Katsube and Collett (1971)—breccia sample 10065; 5. Katsube and Collett (1971)—fines sample 10084; 6. Gold et al (1971)—fines, various densities. The frequency range to be used in the Surface Electrical Properties Experiment on Apollo 17 is marked 'S.E.P.'

of a few meters to a few kilometers are characteristic. However, it is not feasible now to build a tuned sweep-frequency antenna that gives interpretable results over our frequency band of interest; thus, we restrict ourselves to the variation of distance of a few fixed frequencies.

Two criteria must be met for the RFI method to effectively detect and determine depth of a subsurface boundary. First, the dielectric medium must have a loss tangent less than about 0.1, or the amplitude of the waves that travel in the medium will be too low to interfere well with the direct wave—i.e., the medium probed must be transparent at the frequency used. Second, there must exist a contrast in electrical or magnetic properties below the surface in order to reflect energy.

Several waves are generated which are im-

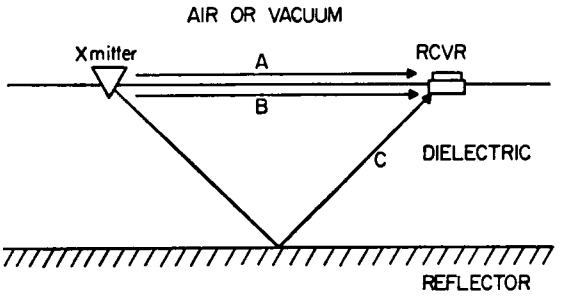

FIG. 2. The basic interferometry concept. The interference of the direct waves A and B and the reflected waves C is measured at the receiver.

portant near the source. Their geometric relations are illustrated in Figure 3. Two spherical waves, A and C, travel directly between the transmitter and the receiver. Wave C travels in the upper medium (air or vacuum), and wave A, in the earth. Since these waves have different velocities, they will interfere with each other. This interference gives a measure of the dielectric constant of the lower medium, since the greater the difference in the velocities of these two waves, the greater will be the interference frequency.

The flank, head, or lateral wave B and the spherical wave A give the transmitting antenna a highly directional radiation pattern. The lateral wave satisfies the boundary conditions imposed by wave C at the interface, since the horizontal phase velocity of B in the earth is the same as that of wave C in the upper medium. To have the same horizontal phase velocity, wave B propagates downward at an angle β as shown in Figure 3. This angle is the angle of total internal reflection between the two media familiar to seismologists, defined by

$$\sin \beta = \sqrt{\frac{\epsilon_0}{\epsilon_1}}, \tag{1}$$

where the critical angle β is the angle between the negative z-axis and the direction of propagation of wave B, and ϵ_0 and ϵ_1 are the dielectric constants of the upper and lower media, respectively (assuming nonmagnetic media). The amplitudes of A and B are largest in the direction β. This feature is important in RFI depth sounding since energy is preferentially transmitted downward at an angle β.

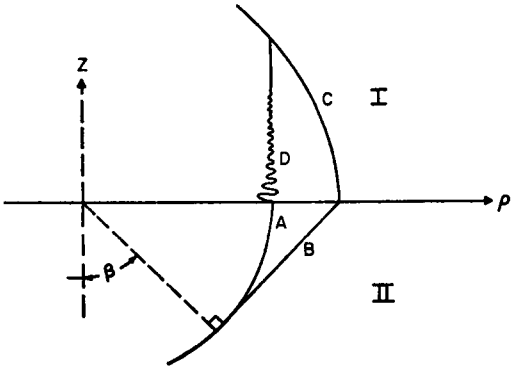

FIG. 3. Wavefronts at the air-dielectric ($z=0$) boundary. ρ is the radial direction from the source. Medium I is air or vacuum (ϵ_0, μ_0), and medium II is a dielectric (ϵ_1, μ_1). A is a spherical wave propagating radially in medium II; B is a head wave propagating downward at the critical angle; C is a spherical wave propagating radially in medium I; and D is an inhomogeneous wave propagating radially in medium I, but attenuating exponentially with height.

The spherical wave A, traveling in the lower medium, also has a complementary wave which matches the boundary conditions. An inhomogeneous wave D is produced at the surface; this wave propagates radially from the source with the velocity of A, but decays exponentially with height above the surface. This wave is significant near the boundary, but its effect decreases as the receiver moves away from the surface.

A "critical distance" r_c is defined as

$$r_c = 2d \tan \beta, \tag{2}$$

where d is the depth to a plane horizontal reflector. Three general regions exist: the near-field, where the transmitter-receiver distance is much less than r_c; the region near the critical distance, where the bulk of the reflected energy arrives; and the far-field, well beyond r_c. In the near-field

the interaction between the two spherical waves A and C dominates and can be used to measure the dielectric constant of the upper layer. As the transmitter-receiver distance approaches r_c, several different waves with roughly comparable magnitudes arrive and produce a very confusing interference pattern. In the far-field, multiple reflections are important, and only the normal modes of the system propagate with low attenuation.

From data obtained in the three regions, three pieces of information can be determined. The *dielectric constant* is related simply to the spatial frequency in the near-field. The *depth* to an interface can be roughly estimated from the dielectric constant and the critical distance. Third the shape of the curve and the number of far-field peaks are indicative of the *loss tangent* of the upper layer.

Two different configurations of equipment have been used in our tests; namely, horizontal electric dipole sources with magnetic dipole receivers for field work, and a vertical magnetic dipole source with an electric dipole receiver for early analog scale-model studies. Both horizontal electric and vertical magnetic dipoles produce horizontally polarized waves. Since the E-field polarization is then perpendicular to the plane of incidence, the reflection coefficient does not go through the Brewster angle null, which is associated only with waves polarized in the plane of incidence on the assumption of nonmagnetic materials.

The general configuration and notation used are shown in Figure 4 for the electric dipole. The dipole is on the surface, extends along the x-axis, and traverses are run orthogonal to it. For this configuration, approximate theoretical solutions for components H_z (vertical magnetic field), H_ρ (radial magnetic field), and E_ϕ (tangential electric field) have been found. The other components are negligible for the case of infinite horizontal plane boundaries. Nonmagnetic materials have been assumed throughout so that $\mu_0=\mu_1=\mu_2$.

Three cases involving infinite plane horizontal layers have been studied theoretically:

(a) the half-space;

(b) the two-layer earth with a perfect reflector at some depth; i.e., either $\epsilon_2\rightarrow\infty$ or tan $\delta_2\rightarrow\infty$ so that the reflection coefficient of the lower boundary is always unity;

(c) the general two-layer earth in which $\epsilon_1\neq\epsilon_2$ and tan $\delta_1\cong$tan δ_2. For the experimental results, the material properties are such that only cases (a) and (b) need to be considered. Theoretical computations are compared with both scale-model and glacier field data. First, however, a brief description of the scale model and the field tests will be given.

ANALOG SCALE MODEL

Scaling of an electromagnetic model is particularly simple when the conductivity is negligible. The wavelength is inversely proportional to the frequency used, and all other relations remain invariant. In our scale model, we used microwave frequencies with free-space wavelengths of 3 to 5 cm. By scaling all data in terms of wavelengths, model, field, and theoretical results can readily be compared.

The first scale model consisted of a klystron source at 10 Ghz feeding a vertical magnetic slot antenna, a small diode receiver, a traversing system, and an automatic recording arrangement. The dielectric used was dry, pure quartz sand (160 mesh), and the reflector was an aluminum plate. The plate and sand were contained in a plywood box with sides that sloped out at about 45 degrees. The box was approximately 30 wavelengths long and 15 wavelengths wide, at the bottom. The setup is shown schematically in Figure

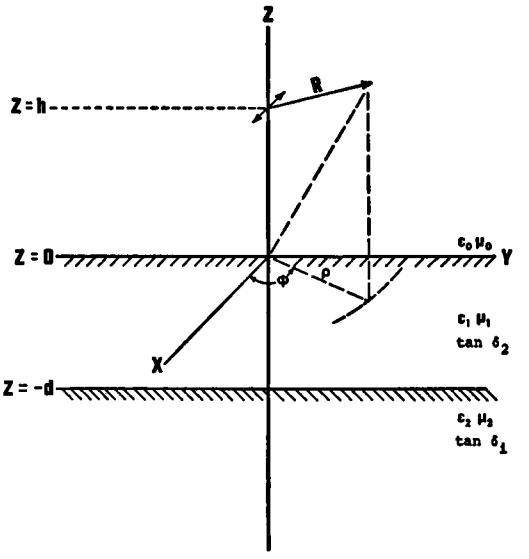

FIG. 4. General configuration of a horizontal electric dipole over a two-layer earth. ϵ_i is the real dielectric constant, μ_i is the permeability, and tan δ_i is the loss tangent of the ith layer.

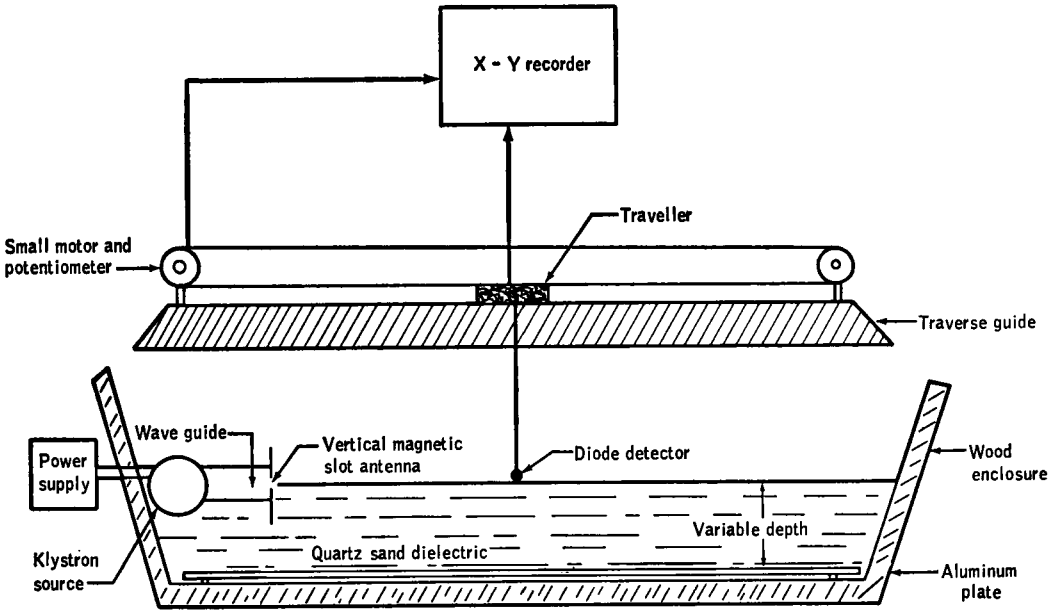

FIG. 5. The analog scale model. The transmitter was composed of a klystron tube radiating at 10 GHz into a rectangular waveguide. A vertical magnetic slot antenna was formed by a slit at the end of the waveguide. The transmitter could be raised or lowered. Signals were received by a small diode which could traverse for about 20 wavelengths at any height. The dielectric used was quartz sand and the reflector was a flat aluminum plate. Received signal strength versus receiver position was recorded directly on an X–Y recorder.

5. A later version of the scale model using transformer oil as a liquid dielectric has also proved very successful. The transmitter and receiver were small electric dipoles, operated at 6 Ghz, and the model was contained in a tank lined with microwave absorbing material.

The validity of our experimental arrangement was initially tested by comparing model results with theoretical predictions for a very simple case. The transmitter and receiver were both placed at height h above the aluminum plate without the sand.

From Part I, the EM radiation from a vertical magnetic dipole at height h over a magnetically uniform half-space is described completely by the vertical magnetic Hertz vector, given by

$$\pi_z = \frac{e^{ik_0R}}{R} + R_{01}\frac{e^{ik_0R'}}{R'}, \qquad z \geq 0, \quad (3)$$

where k_0 is the wavenumber, R_{01} is the reflection coefficient at the boundary ($z=0$), R is the direct distance to the receiver, and R' is the distance traveled by the reflected wave. If the boundary is a perfect reflector, $R_{01}=-1$. For the receiver at height h:

$$R = [r^2 + (z-h)^2]^{\frac{1}{2}} = r, \quad (4)$$

and

$$R' = [r^2 + (z+h)^2]^{\frac{1}{2}} = [r^2 + 4h^2]^{\frac{1}{2}}. \quad (5)$$

The tangential electric field E_ϕ is then

$$\begin{aligned} E_\phi &= -i\omega\mu\frac{\partial \pi_z}{\partial r} \\ &= -i\omega\mu\left[\frac{e^{ik_0r}}{r}\left(ik_0 - \frac{1}{r}\right)\right. \\ &\quad - \frac{e^{ik_0\sqrt{r^2+4h^2}}}{\sqrt{r^2+4h^2}}\left(ik_0 - \frac{1}{\sqrt{r^2+4h^2}}\right)\cdot \\ &\quad \left.\left(\frac{r}{\sqrt{r^2+4h^2}}\right)\right]. \end{aligned} \quad (6)$$

Then,

$$\begin{aligned} E(r,h) = A\left[\frac{e^{ik_0r}}{r}\left(i - \frac{1}{r}\right) - \frac{e^{i\sqrt{r^2+4h^2}}}{\sqrt{r^2+4h^2}}\right. \\ \left.\cdot\frac{r}{\sqrt{r^2+4h^2}}\left(i - \frac{1}{\sqrt{r^2+4h^2}}\right)\right], \end{aligned} \quad (7)$$

where $A = -i\omega\mu(4\pi^2/\lambda^2)$ and is an arbitrary scaling factor for a unit magnetic dipole, r is the transmitter-receiver separation in wavelengths, h is the transmitter-receiver height above the reflecting plate in wavelengths, and λ is the wavelength in free-space.

Typical comparisons between theory and experiment are shown in Figure 6. The agreement in the position of the peaks is very good. Although the amplitudes are on an arbitrary scale and are therefore not directly comparable, the ratio between each theoretical and experimental peak is approximately constant. Experimental deviations from theoretical solutions are not large and are primarily due to reflections between the transmitter and either the receiver or the sides of the box. The good agreement between calculated and measured curves was taken as the main proof that the experimental arrangement was satisfactory to measure interference between various waves.

GLACIER FIELD TESTS

Introduction

Ice is one of the few terrestrial rocks with uniformly high resistivity. Resistivities of 10^5 to 10^7 ohm-m have been measured consistently (e.g., Röthlisberger, 1967; Keller and Frischknecht, 1961). A few glaciers have been carefully mapped and are accessible for field tests. We selected two on which to test the RFI technique.

The dielectric properties of ice and snow have been reviewed by Evans (1965). The dielectric properties of glacial ice and snow have been studied in situ by Watt and Maxwell (1960) and by Walford (1968). Two parameters are important —the dielectric constant and the loss tangent. Ice has a relaxation in the audio-frequency range, but unlike many dielectric materials has none near the radio frequencies. Hence, while the value of its dielectric constant is frequency independent in the radio frequencies, the value of its loss tangent is roughly inversely proportional to frequency and is strongly temperature dependent.

From 1 to 30 Mhz, the value of the dielectric constant is 3.20 ± 0.05 and is fairly independent of frequency, impurities, or temperature. Over the same frequencies, $f \cdot \tan \delta \cong 0.25$ at 0°C, but $f \cdot \tan \delta \cong 0.10$ at -10°C, where f is the frequency in Mhz. Although the effects of impurities, cracks, air bubbles, and free water on the loss tangent are not well understood, the values for losses in gla-

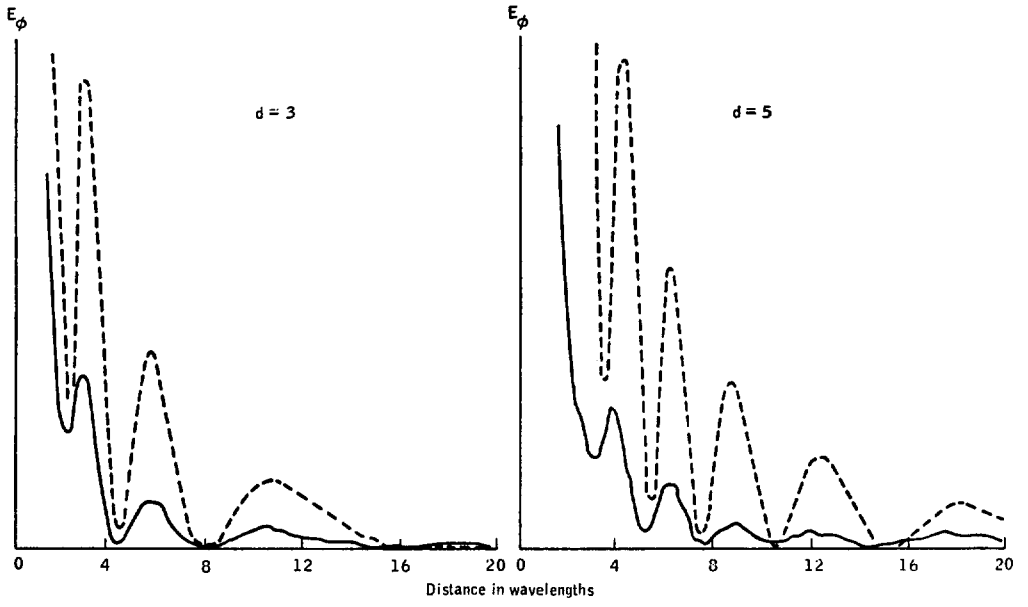

FIG. 6. Typical theoretical and experimental curves for calibration of the scale model. Dashed line is theoretical and solid line is scale model. Curves for a depth of 3 wavelengths are on the left, and for 5 wavelengths, on the right. No dielectric is present. Scaling is different for each of the four curves.

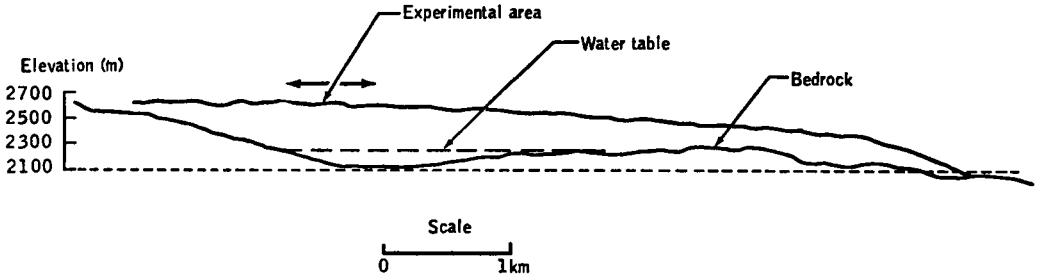

FIG. 7. Cross-section of the Gorner Glacier, from Swiss seismic data.

cier ice are not appreciably different from those in pure ice.

The inverse-frequency dependence of the loss tangent in ice implies that the attenuation of an EM wave in ice is directly proportional to the absolute distance, not to the number of wavelengths that the wave travels. Therefore, the maximum sounding depth in ice free of scattering bodies is virtually independent of the frequency used by any radio or radar technique in the frequency range from 0.1 to nearly 1000 Mhz.

The Gorner Glacier

The Gorner Glacier, located in southern Switzerland, has been extensively drilled and mapped seismically for the Swiss Hydroelectric System, and a longitudinal section of the glacier is shown in Figure 7. It is a deep glacier; the depth in the test area to the postulated water-table is about 400 m and the depth to bedrock is 500 m. It is effectively a half-space for the interferometry technique.

Equipment used on the tests, run in September, 1969, was both simple and portable. The transmitter was a General Radio 1330A bridge oscillator, which fed the transmitting antenna through a ferrite core 1 to 1 balun. Two types of transmitting antennas were used: an untuned horizontal electric dipole and a small ($\lambda/10$ diameter) loop as a vertical magnetic dipole. Output power was less than $\frac{1}{2}$ watt. The receiver was fed by either a 5-m electric dipole or a Singer single-turn 1-m diameter loop, with simple broad-band matching to the 50-ohm input impedance of a Galaxy R530 communications receiver. The receiver output was read from a Hewlett-Packard 427A portable voltmeter and recorded manually.

Field procedure consisted of recording field strength about every $\frac{1}{4}$ wavelength along traverses away from the transmitter. Frequencies of 1, 2 4, 7, and 10 Mhz were used. E_ϕ, H_z, and H_ρ components were measured for both horizontal electric and vertical magnetic transmitting antennas.

The Athabasca Glacier

The Athabasca Glacier, located in Alberta, Canada, has also been studied extensively: a gravity survey has been conducted by Kanasewich (1963), seismic and drilling studies have been made by Paterson and Savage (1963), and EM and resistivity soundings have been run by Keller and Frischknecht (1961). A depth contour map, reconstructed from Paterson and Savage and showing our traverse line, is given in Figure 8. The thickness of the ice along the traverse varies from about 130 m to 280 m.

The Athabasca Glacier tests, run in March, 1970 used a crystal-controlled transmitter that was operated at frequencies of 2, 4, 8, 16, and 24 Mhz. Output power was about one watt. It fed a ribbon-wire tuned horizontal electric dipole antenna through a balun feed network. The antenna consisted of several number-22 wires, each cut to the resonant length for a single frequency, lying beside each other on the ice surface. Each wire was cut to the resonant length of one of the frequencies in free space and connected in parallel to the balun feed. Each wire had to then be cut to between 75 and 90 percent of its length in order to reflect minimum power back to the transmitter.

This antenna was experimental, and several problems may have been associated with its use. The amount of clipping needed to retune the wires after they had been placed on the ice was insufficient to account for the dielectric contrast between ice and air. We feel that each wire was

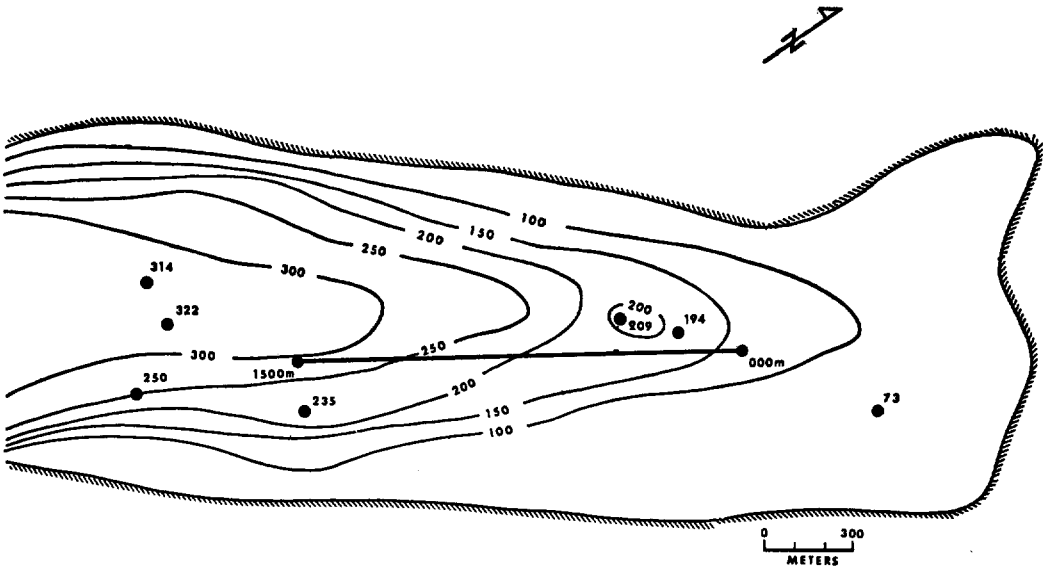

FIG. 8. Contour map of the Athabasca Glacier, drawn from the seismic and drilling data of Paterson and Savage (1963). Boreholes, with depths in meters, are shown. Our interferometry traverse line is marked 000 m to 1500 m.

reactively coupled to the other wires, which then radiated energy. Therefore, the longer wires were effectively long antennas (greater than a half wavelength) for the higher frequencies and could have radiated significantly off the orthogonal direction. The antenna was probably not well coupled either to the subsurface or to the traverse direction, and spurious reflections could have been received from the sides of the glacier.

The receiver and the field procedure were similar to those used on the Gorner Glacier with the following differences: A smaller $\frac{1}{3}$-m-diameter loop was used for 16 and 32 Mhz. Readings were taken every $\frac{1}{6}$ wavelength, to a distance of 20 wavelengths or until the signal was too low to detect. Most traverses were run from NE to SW, although a few were run from SW to NE with the transmitter displaced to the SW end of the traverse line. Both H_z and H_ρ components were taken, as well as one E_ϕ traverse.

RESULTS

The half-space

If the boundary between the first and second layers is not important, the only waves which reach the receiver are the direct waves through the air (or vacuum) and the dielectric. This case is simple to solve theoretically, and suites of curves have been compiled for the E_ϕ, H_ρ, and H_z components (see, for example, Figure 9). There is very good agreement between theory and experimental results from the Gorner Glacier. Figure 10 shows a typical experimental curve and a series of theoretical curves for various dielectric constants. The interference peaks and troughs align best with those calculated for $\epsilon_1 = 3.2$. By comparison with curves like those in Figure 9, we have estimated the loss tangent to be less than 0.07 at 10 Mhz.

One interesting feature of both the theoretical and experimental half-space curves is that results for the H_z and E_ϕ components are identical, but the peaks and troughs of the H_ρ component are shifted $\frac{1}{2}\lambda$ away from the transmitter (see Figure 11). This relation between the interference patterns in H_z, E_ϕ, and H_ρ provides a basis on which to detect departures of the fields from the half-space response which could be due to subsurface reflections or scattering from surface or subsurface irregularities.

Therefore, in a half-space, RFI can easily be used to determine the dielectric constant of the upper layer if we know the positions of the peaks and troughs. Theoretical results indicate that the

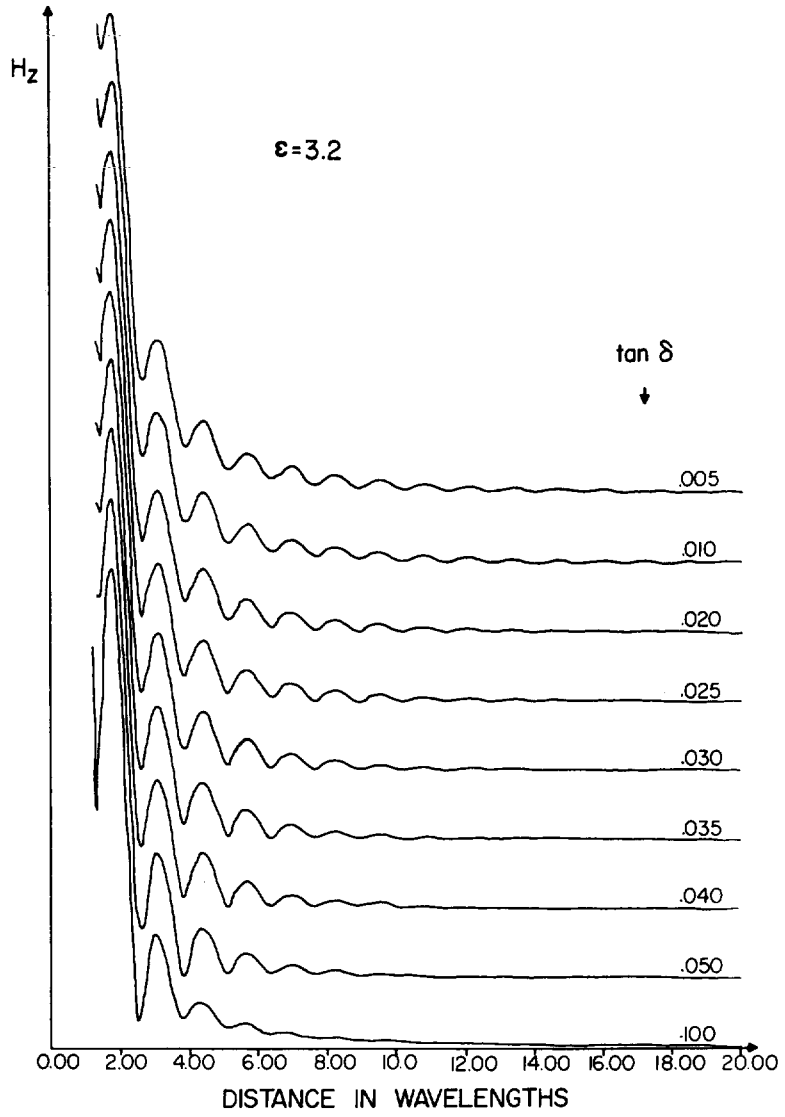

FIG. 9. Theoretical half-space curves for a dielectric constant of 3.2 and various loss tangents. Peaks and nulls, are less distinct for higher loss tangents, but their positions do not change.

loss of the layer does not change the position of the peaks, but as the loss decreases, both the sharpness of the nulls and the number of observable peaks increases. By measuring several components it may be possible to determine if the measurements have been affected by random scattering.

Two-layer earth: Perfect reflector

Calculations for the two-layer model are more complex. Exact theoretical solutions have not been obtained, but after performing the mathematical manipulations discussed in Part I, approximate numerical solutions have been compiled and plotted. Typical suites of curves are shown in Figure 12 to illustrate the effect of changes in dielectric constant, thickness, and loss tangent, of the first layer. Although the effects of these parameters are not fully separable, in general, the frequency of the initial peaks and troughs is indi-

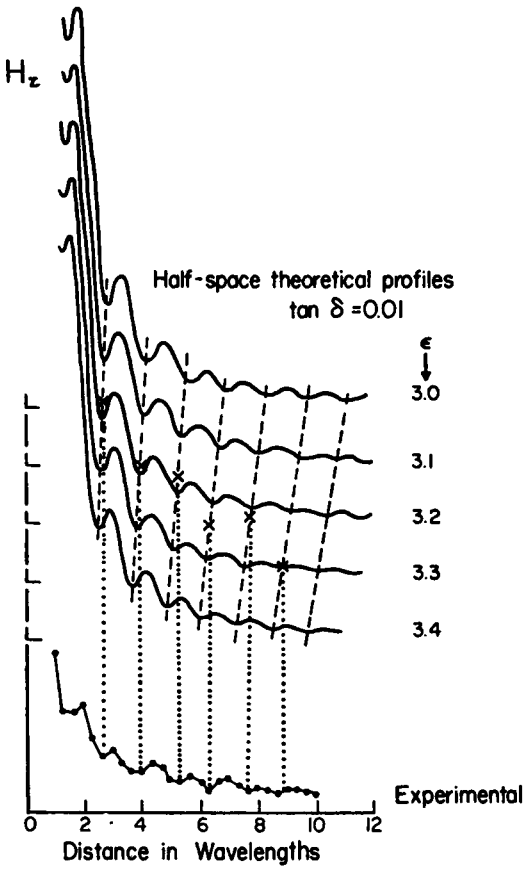

FIG. 10. Several theoretical half-space curves and an experimental curve from the Gorner Glacier at 10 Mhz (H_z component). The experimental curve has peaks and troughs that correspond to the theoretical curve for a dielectric constant of 3.2.

cative of the dielectric constant; the position of the main energy peak is determined by the thickness and the dielectric constant; and the sharpness of the pattern changes with the loss tangent. For this example, the dependence on loss tangent is particularly noticeable for loss tangents in the range .01 to .05.

A suite of analog scale-model patterns and the corresponding theoretical curves are shown in Figure 13. The dielectric oil had a measured dielectric constant of 2.16 and a loss tangent of 0.0022. In general, for thicknesses greater than 2 or 3 wavelengths the agreement in both position and amplitude of the peaks and nulls is good. For thinner layers the agreement is poorer, probably because the theoretical solutions become less accurate (see Part I). Differences between experimental and theoretical results in the near-field may also be caused by the theoretical approximations. They might also be caused by spurious reflections in the experimental tank from wires connecting the transmitting antenna to its source. The other major discrepancy between the two solutions is at the critical angle where the approximations made in the theory are most significant. However, the good agreement between theoretical and scale-model results has given us confidence in both.

The results from the Athabasca Glacier are complicated by the fact that the thickness of the glacier increases along the traverse with a slope of approximately 1:10. Since the general theory for this geometry is extremely difficult, and has not been worked out in detail, we used theoretical curves for several thicknesses near the mean traverse thickness for comparison. Such a comparison is not altogether accurate, since the effects of a thickening layer depend on both the thickness and the rate of change of thickness.

Comparisons were made between data measured on the Athabasca Glacier and many suites of theoretical curves. It was found that the family of theoretical curves for the known parameters of the glacier, when compared with the experimental data as a whole, fitted better than any other set, although there was some ambiguity. Several examples are shown in Figure 14. The experimental data were run through a simple 1, 1, 1 running average filter before plotting. This filtering enhanced the main features of the curves by reducing small random variations. The agreement between theoretical and experimental data is far from perfect. However, if it is recognized that because the thickness of the ice is increasing along the traverse, some moveout of the measured peaks is to be expected, and a consistent picture emerges.

Figure 14 shows data obtained at 2, 4, 8, and 24 Mhz on the Athabasca Glacier, along with three theoretical curves with depths bracketing those along the traverse. As the frequency increases, the thickness of the ice, measured in wavelengths, also increases, so that quite different curves are found for each frequency. At 2 Mhz the curves are smooth and regular and the agreement between theory and experiment is quite good. At 4 Mhz the patterns are more complex, and although these are similar features, the the-

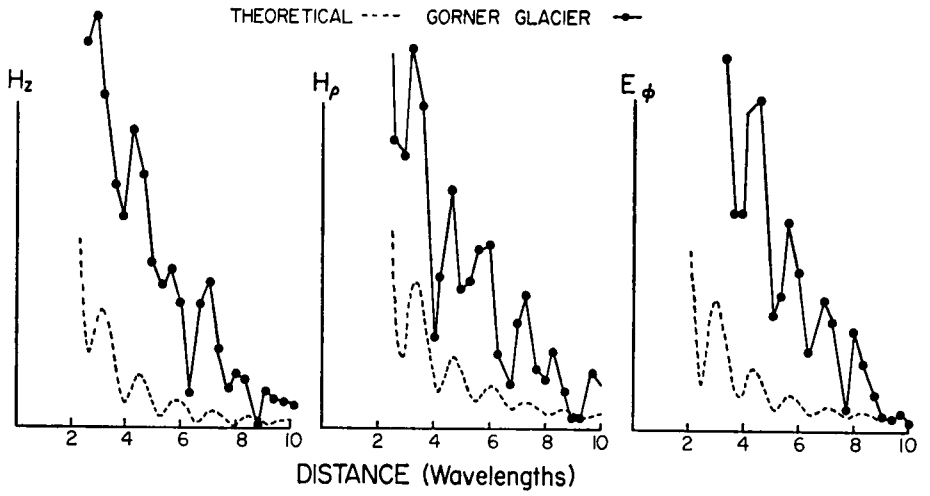

FIG. 11. Theoretical half-space curves and results from the Gorner Glacier. Source is a horizontal electric dipole at 10 Mhz. Theoretical curves are for dielectric constant of 3.2 and a loss tangent of 0.03. Peaks and troughs for the $H\rho$ component are shifted away from the transmitter one-half wavelength.

oretical curves do not correspond exactly to the experimental. At 8 Mhz the curves are complex, but the agreement is better, especially the large peak at about 7 wavelengths distance. At 24 Mhz there are many peaks and troughs in both curves. We feel the lack of correlation between theory and experiment is largely due to many randomly scattered reflections in the experimental curve. At 24 Mhz the wavelength of 12.5 m is the same size as many crevasses and surface roughness features.

In summary, as the thickness of the dielectric layer increases, the interference patterns change from curves with a few well-defined peaks to curves with high spatial frequencies and no large peaks. These features are seen in both theoretical and experimental results. The fact that both H_ρ and H_z components are basically similar, although they differ in their fine structure, increases our confidence in the match between theory and experiment.

INTERPRETATION

Dielectric constant

This parameter is easy to obtain directly from the data, since, as shown above, the direct air and subsurface waves interact near the source to give a pattern dependent only on this parameter. If the air wave has a wavenumber k_0,

$$k_0 = \frac{2\pi}{\lambda_0}, \tag{8}$$

where λ_0 is the free-space wavelength; and if the subsurface wave has wavenumber k_1,

$$k_1 = \frac{2\pi}{\lambda_1} = \frac{2\pi\sqrt{\epsilon_1}}{\lambda_0} = \sqrt{\epsilon_1}\, k_0, \tag{9}$$

then the beat frequency wavenumber k is

$$\Delta k = k_1 - k_0 = \frac{2\pi}{\lambda_0}(\sqrt{\epsilon_1} - 1). \tag{10}$$

The spatial interference wavelength λ_b is then

$$\lambda_b = \frac{2\pi}{\Delta k} = \frac{\lambda_0}{\sqrt{\epsilon_1} - 1}. \tag{11}$$

Therefore,

$$\epsilon_1 = \left(\frac{\lambda_0}{\lambda_b} + 1\right)^2 \tag{12}$$

and can be obtained directly from the data. For ice, $\lambda_b \cong 1.27\lambda_0$.

Loss tangent

The loss tangent can be estimated in a qualitative way from the sharpness of the patterns in the

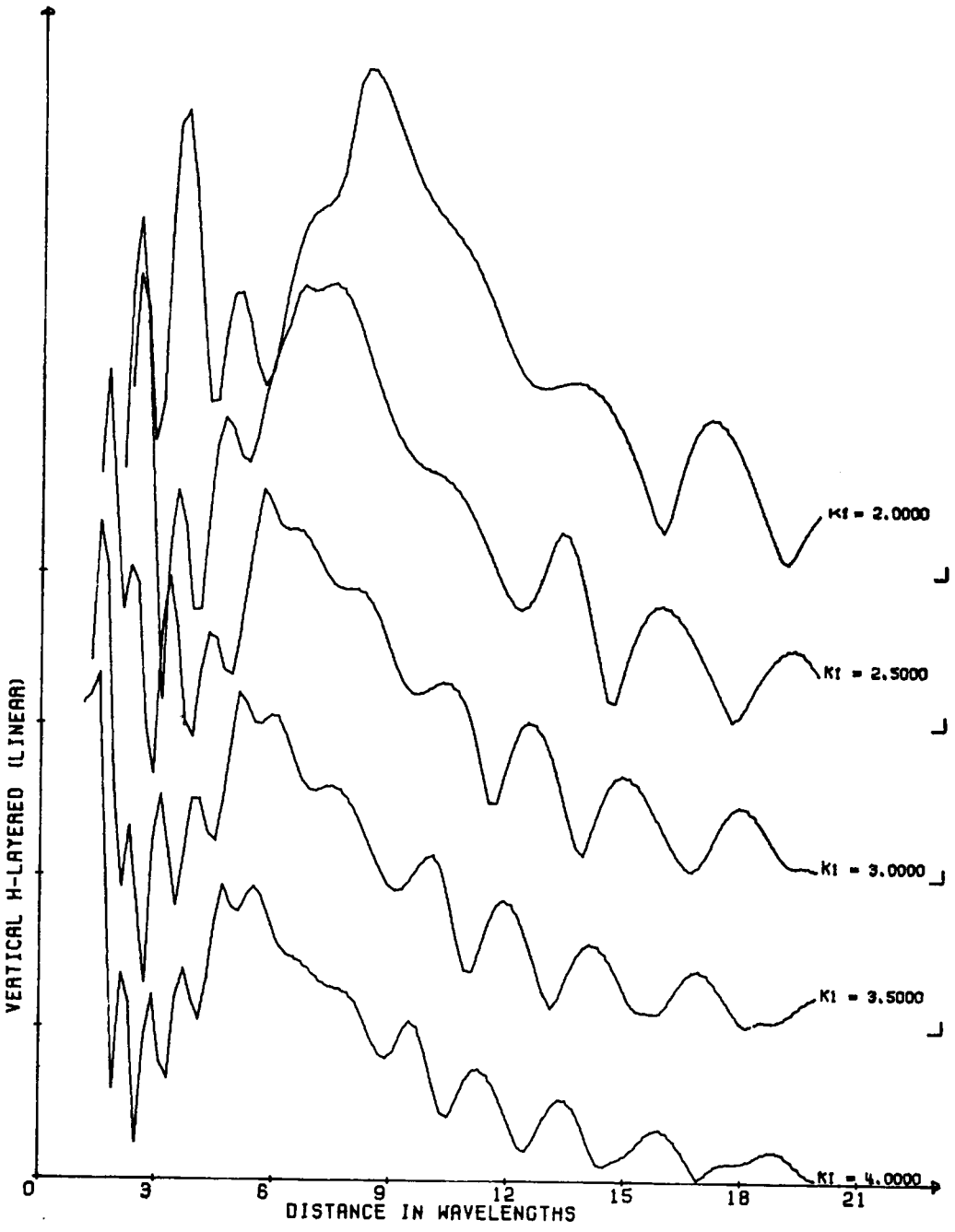

Fig. 12a. Theoretical interference curves for H_z component over a two-layer earth. Dependence on dielectric constant is shown. Depth = 4.000 λ, LT1 = 0.0200, K1 = varying.

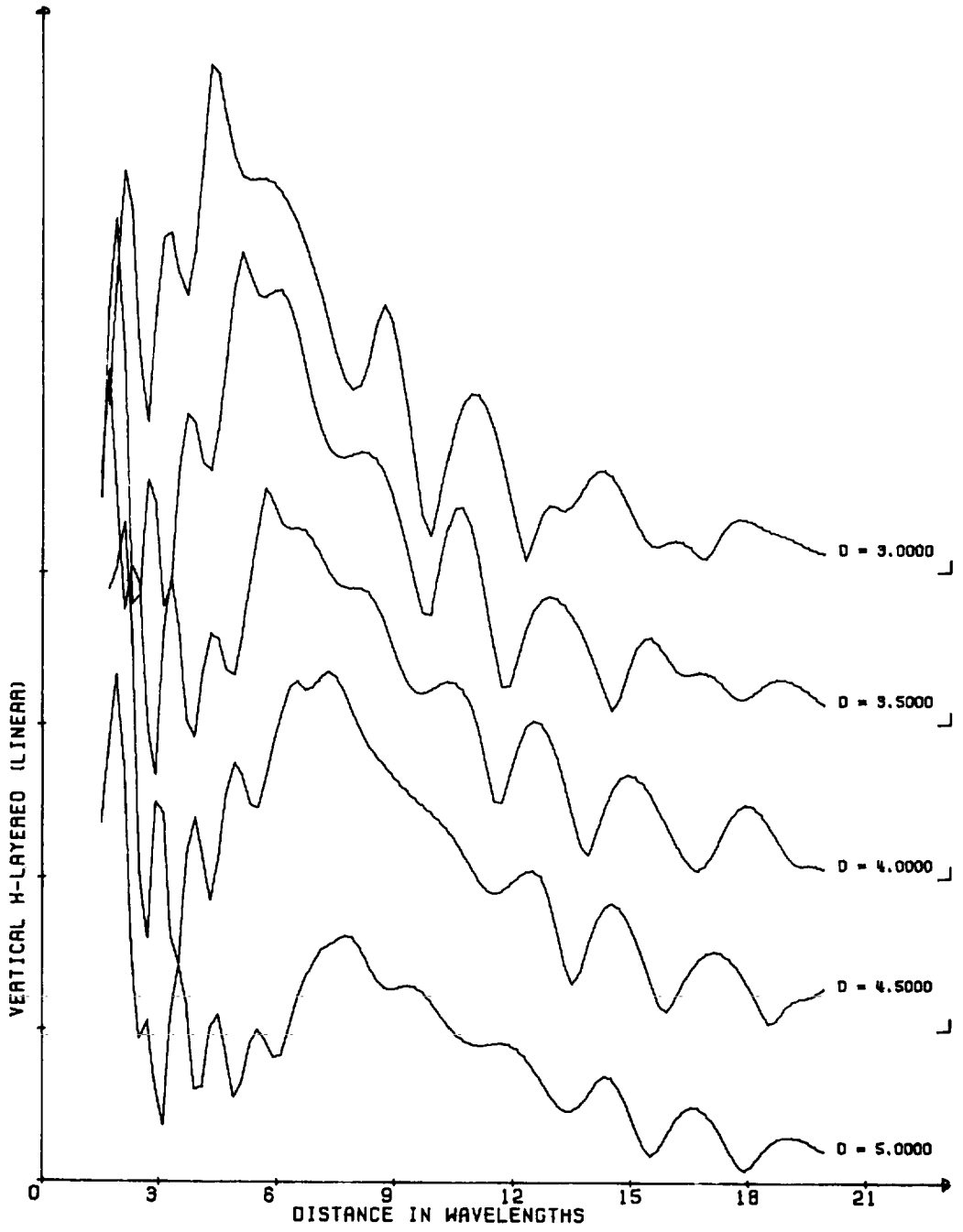

Fig. 12b. Theoretical interference curves for H_z component over a two-layer earth. Dependence on thickness is shown. Depth = varying, LT1 = 0.0200, K1 = 3.000.

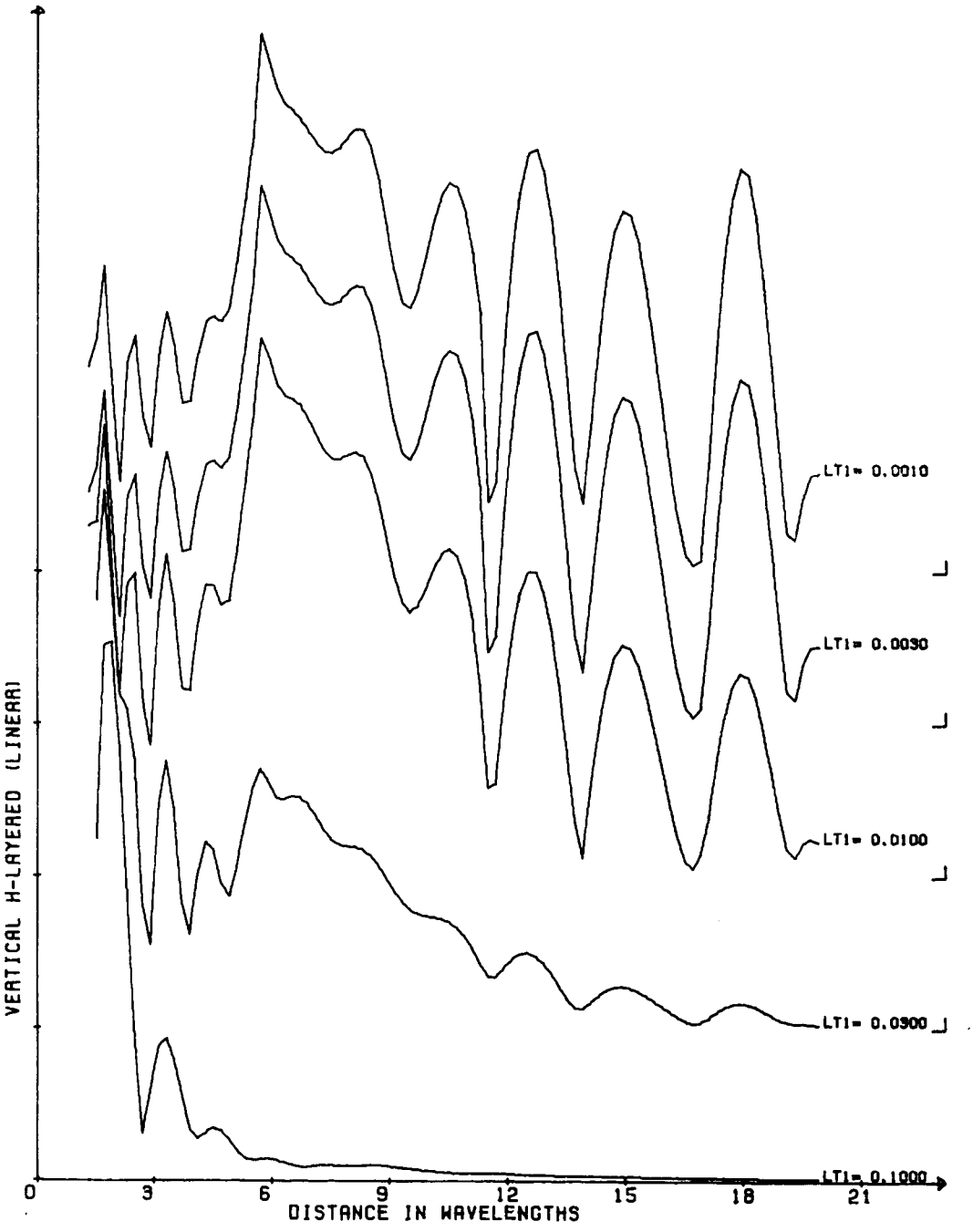

FIG. 12c. Theoretical interference curves for H_z component over a two-layer earth. Dependence on loss tangent is shown. Depth = 4.000λ, LT1 = varying, K1 = 3.000.

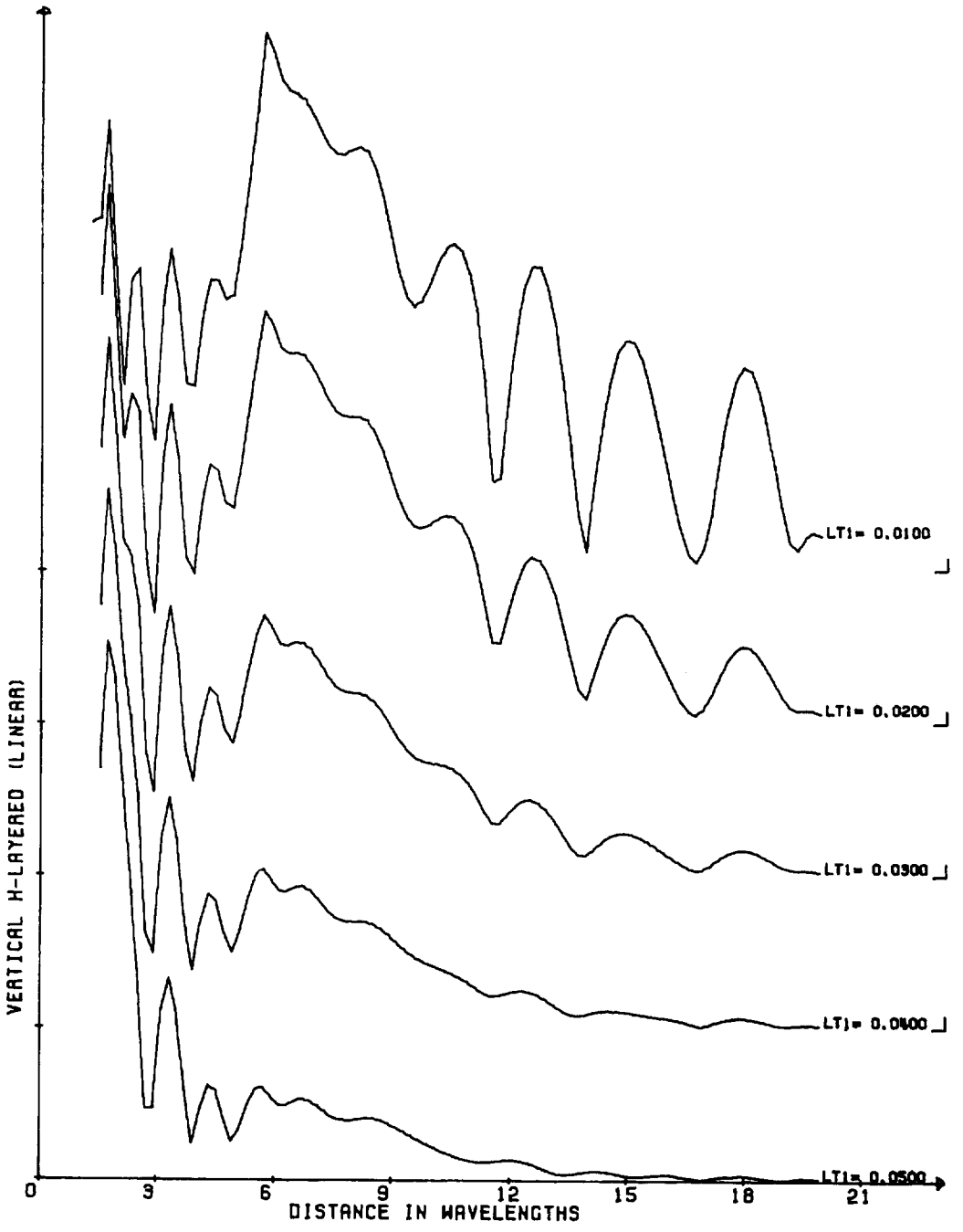

FIG. 12d. Theoretical interference curves for H_z component over a two-layer earth. Dependence on loss tangent is shown. Depth=4.000 λ, LT1=varying, K1=3.000.

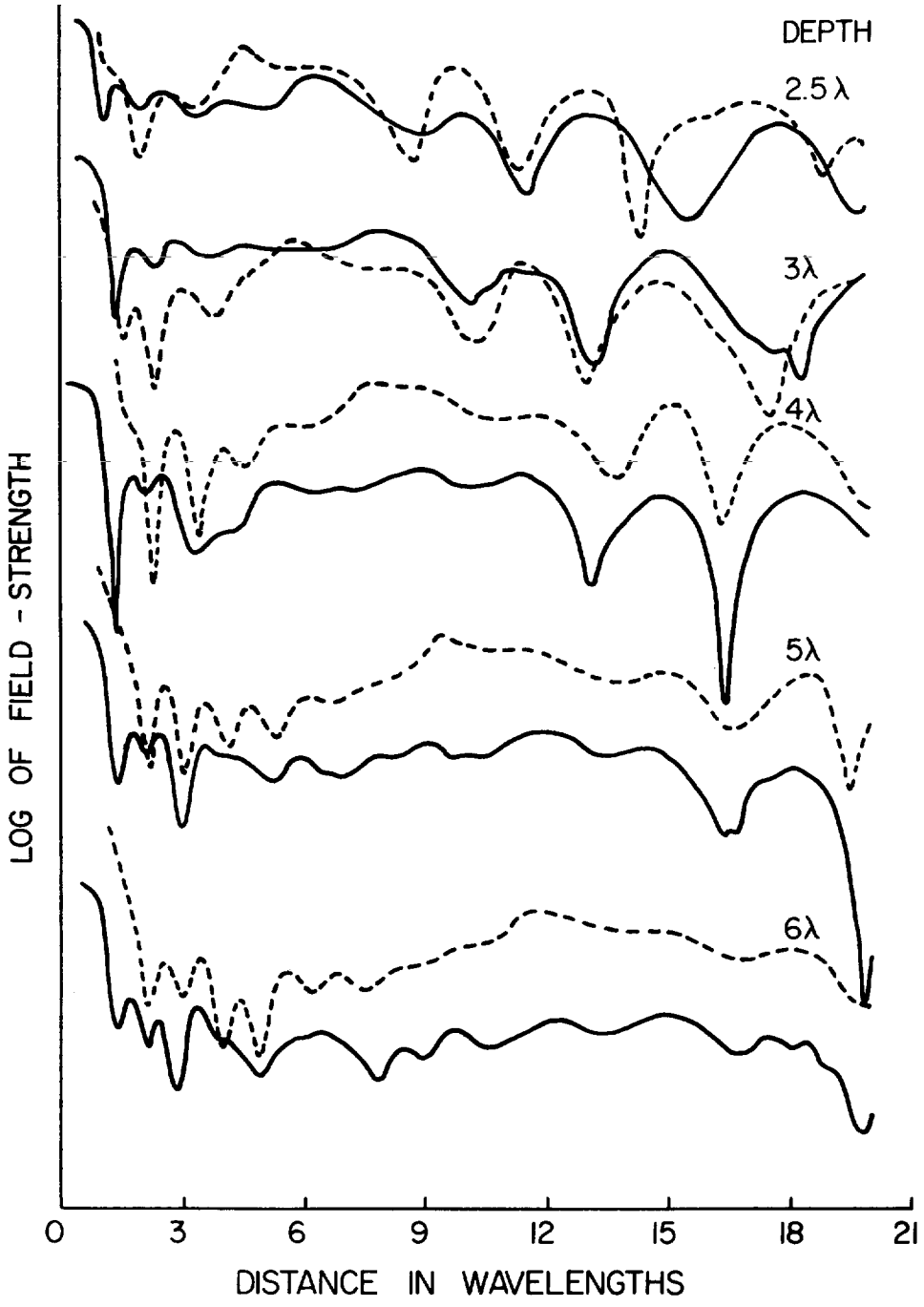

FIG. 13. Analog scale-model curves (solid line, E_θ) and corresponding theoretical curves (dashed line, H_z, $K=2.16$, $\tan\delta=.0022$) for various thicknesses of the upper layer. E_ϕ and H_z are identical in this configuration. Dielectric constant (K) and loss tangent ($\tan\delta$) were measured independently.

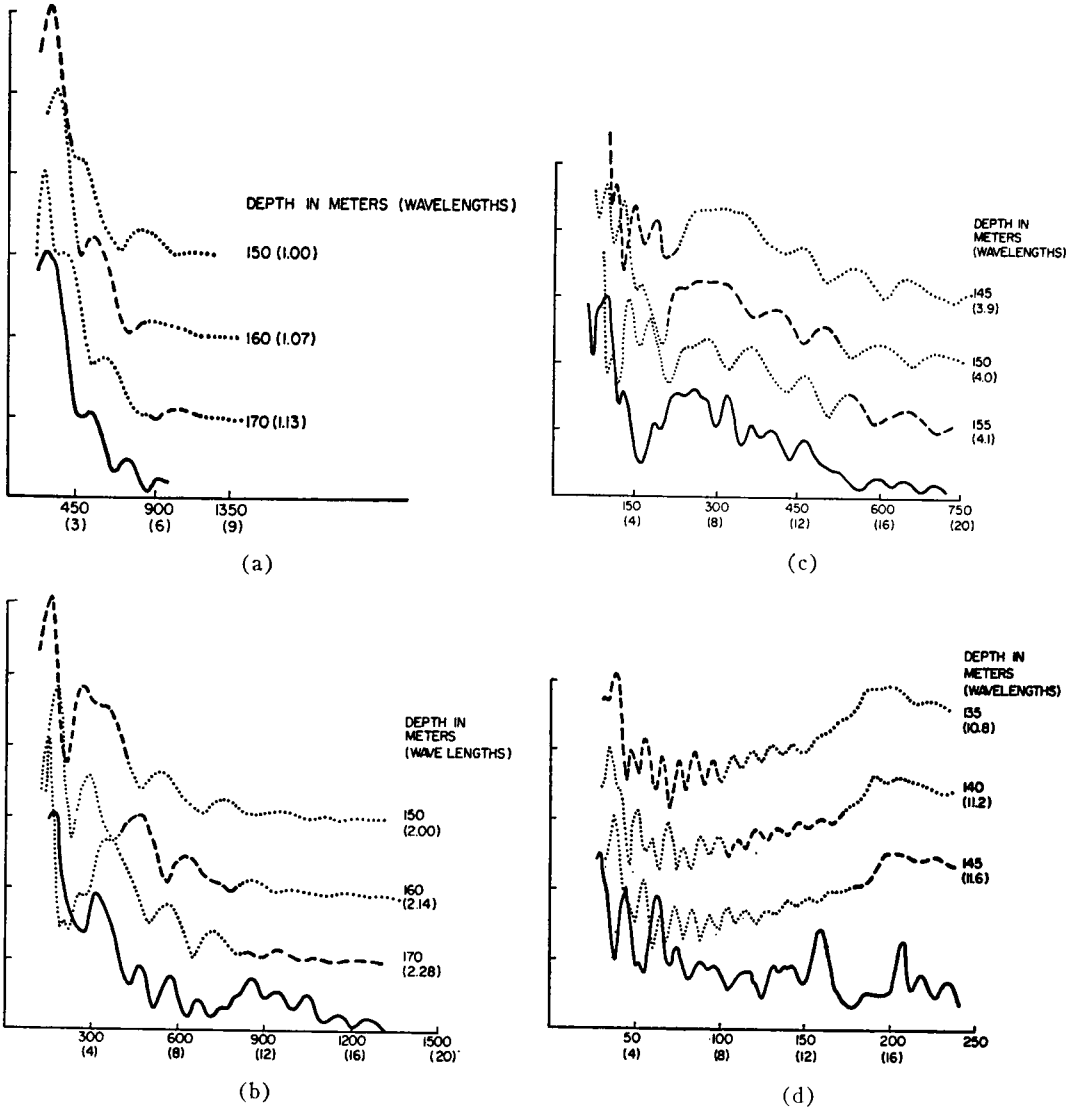

FIG. 14. Theoretical curves and Athabasca Glacier results at (a) 2, (b) 4, (c) 8, and (d) 24 Mhz. (a) dashed/dotted line, theoretical H_z, $K=3.2$, tan $\delta=0.08$; solid line, experimental Athabasca Glacier, H_z, 2 Mhz. (b) dashed/dotted line, theoretical $H\rho$, $K=3.2$, tan $\delta=0.04$; solid line, experimental Athabasca Glacier, $H\rho$, 4 Mhz. (c) dashed/dotted line, theoretical $H\rho$, $K=3.2$, tan $\delta=0.02$; solid line, experimental Athabasca Glacier, $H\rho$, 8 Mhz. (d) dashed/dotted line, theoretical H_z, $K=3.2$, tan $\delta=0.007$; solid line, experimental Athabasca Glacker, $H\rho$, 24 Mhz. Distance in meters (wavelengths).

near field. In the near field the two direct waves add to form peaks and subtract to form nulls. If the waves are about the same size, the peaks and nulls will be sharp, but if one wave is much larger than the other, there will be little interference.

As the amplitude of the subsurface wave decreases below the amplitude of the air wave, the pattern becomes less sharp. An envelope formed by joining the peaks and by joining the nulls of the interference pattern becomes thinner at a rate determined by the loss tangent of the medium.

In the Gorner Glacier data, the loss tangent was estimated to be less than 0.7/f (Mhz), well

within the published value for ice. In the Athabasca data, reflections appear to disturb the two direct waves too greatly to be able to use this simplified approach.

Depth

An estimate of the dielectric constant and the critical distance from the field data can be used to estimate the depth. However, an assumption about the dip of the reflector must be made. The method fails if either the dielectric constant or the critical distance cannot be estimated accurately.

Scattering

One of the major unknowns in the application of the RFI technique is the effect of irregularities in the medium. It is reasonable to believe that the effects of irregular surfaces, inhomogeneities within the dielectric, and objects near the antennas could all perturb the measured data. One possible way to remove small random effects is to appropriately filter the data, and a simple running-average filter was used to enhance the pertinent features of the Athabasca Glacier data.

An estimate of scattering is important to understand geologic structure. During the Athabasca trials the H_ϕ component, which should theoretically be null for plane horizontal layers, was observed to be significant (though weaker than the other components). Therefore, H_ϕ provided a measurement of the scattering, which was considerable at the higher frequencies. The similarity of all the components measured on the Gorner Glacier on the other hand implied that scattering was not significant up to 10 Mhz.

CONCLUSIONS

1. The RFI technique is a practical method with which to study layering in low-loss dielectrics ($\tan \delta < 0.1$).

2. Three parameters of the upper layer can be estimated from the data: the dielectric constant, the loss tangent, and an estimate of the thickness to a reflector. Measurements of $\epsilon = 3.2$ and $f \cdot \tan \delta = 0.7$ (f in Mhz) for ice are in agreement with known results.

3. The method is an inexpensive way to sound ice sheets less than a few hundred meters thick, and could be used to study low-loss layers on the moon.

4. Further work is required to refine and quantify the interpretational procedure, to extend it to more complex geometries, and to understand better the effects of random scatterers.

ACKNOWLEDGMENTS

We would like to acknowledge the assistance of the following: Mr. E. A. Johnston of MIT's Center for Space Research, who built the transmitter used on the Athabasca Glacier and participated in the expedition; Dr. H. Röthlisberger, Mr. P. Fohn, and Mr. M. Aellen, who provided advice on the logistics of the Gorner Glacier; The Department of National and Historic Parks Branch, Calgary, who gave us permission to work on the Athabasca Glacier, and, along with Brewster Transport Company and the Administration of Jasper National Park, provided much useful support; and Dr. A. K. Sinha, who allowed us to use some of his preliminary theoretical curves. We would also like to thank Mr. L. Tsang and Dr. J. A. Kong for pointing out a sign error in programming the theoretical equations.

Financial support was provided by NASA grant no. NGL 22-009-257 and contract NAS9-11540 at MIT with subcontracts at the University of Toronto; Rossiter thanks The Lunar Science Institute, Houston, Texas for support under contract no. NSR 09-051-001.

This work is the second paper in a series providing the background for the Surface Electrical Properties Experiment, planned for the Apollo 17 lunar mission.

REFERENCES

Annan, A. P., 1973, Radio interferometry depth sounding: Part I—Theoretical discussion: Geophysics, this issue.

Chung, D. H., Westphal, W. B., and Simmons, G., 1971, Dielectric behavior of lunar samples: Electromagnetic probing of the lunar interior, *in* Proceedings of the Second Lunar Science Conference: MIT Press, Cambridge, v. 3, p. 2381–2390.

Evans, S., 1963, Radio techniques for the measurement of ice thickness: The Polar Record, v. 11, p. 406–410 and 795.

——— 1965, Dielectric properties of ice and snow—a review: J. Glaciol., v. 5, p. 773–792.

——— 1967, Progress report on echo sounding: The Polar Record, v. 13, p. 413–420.

Gold, T., O'Leary, B. T., and Campbell, M., 1971, Some physical properties of Apollo 12 lunar samples, *in* Proceedings of the Second Lunar Science Conference: MIT Press, Cambridge, v. 3, p. 2173–2181.

Holser, W. T., Brown, R. J. S., Roberts, F. A., Fredriksson, O. A., and Unterberger, R. R., 1972, Radar logging of a salt dome: Geophysics, v. 37, p. 889–906.

Jiracek, G. R., 1967, Radio sounding of Antarctic ice: Res. Rep. No. 67-1, Geophys. and Polar Res. Center, University of Wisconsin.

Kanasewich, E. R., 1963, Gravity measurements on the

Athabasca Glacier, Alberta, Canada: J. Glaciol., v. 4, p. 617–631.
Katsube, T. J., and Collett, L. S., 1971, Electrical properties of Apollo 11 and 12 lunar samples, *in* Proceedings of the Second Lunar Science Conference: MIT Press, Cambridge, v. 3, p. 2367–2379.
Keller, G. V., and Frischknecht, F. C., 1961, Induction and galvanic resistivity studies on the Athabasca Glacier, Alberta, Canada, *in* Geology of the Arctic (International Symposium): edited by G. O. Raasch, Toronto, University of Toronto, v. 2, p. 809–832.
Paterson, W. S. B., and Savage, J. C., 1963, Geometry and movement of the Athabasca glacier: J. Geophys. Res., v. 68, p. 4513–4520.
Röthlisberger, Hans, 1967, Electrical resistivity measurements and soundings on glaciers: Introductory remarks: J. Glaciol., v. 6, p. 599–606.
Saint-Amant, M., and Strangway, David W., 1970, Dielectric properties of dry, geologic materials: Geophysics, v. 35, p. 624–645.
Strangway, D. W., 1969, Moon: electrical properties of the uppermost layers: Sci., v. 165, p. 1012–1013.
Tyler, G. L., 1968, Oblique scattering radar reflectivity of the lunar surface: Preliminary results from Explorer 35: J. Geophys. Res., v. 73, p. 7609–7620.
Unterberger, R. R., Holser, W. T., and Brown, R. J. S., 1970, Radio frequency propagation in salt domes 1. Theory, laboratory and field measurements of attenuation: Presented at SEG 40th Annual International Meeting, New Orleans.
Walford, M. E. R., 1968, Field measurements of dielectric absorption in Antarctic ice and snow at very high frequencies: J. Glaciol., v. 7, p. 89–94.
Watt, A. D., and Maxwell, E. L., 1960, Measured electrical properties of snow and glacial ice: J. Res. U. S. Nat. Bur. Stan., v. 64D, p. 357–363.
Weaver, Harold, 1965, The interpretation of thermal emissivity from the moon, *in* Solar system radio astronomy: edited by J. Aarons, New York, Plenum Press, p. 295–354.